

ALPS: An Auto-Labeling and Pre-training Scheme for Remote Sensing Segmentation With Segment Anything Model

Song Zhang ^{*1} Qingzhong Wang ^{*2}, Junyi Liu ¹, Haoyi Xiong ^{† 2},

¹Aerospace Information Research Institute, Chinese Academy of Sciences. ²Baidu Inc.

Abstract

In the fast-growing field of Remote Sensing (RS) image analysis, the gap between massive unlabeled datasets and the ability to fully utilize these datasets for advanced RS analytics presents a significant challenge. To fill the gap, our work introduces an innovative auto-labeling framework named ALPS (Automatic Labeling for Pre-training in Segmentation), leveraging the Segment Anything Model (SAM) to predict precise pseudo-labels for RS images without necessitating prior annotations or additional prompts. The proposed pipeline significantly reduces the labor and resource demands traditionally associated with annotating RS datasets. By constructing two comprehensive pseudo-labeled RS datasets via ALPS for pre-training purposes, our approach enhances the performance of downstream tasks across various benchmarks, including iSAID and ISPRS Potsdam. Experiments demonstrate the effectiveness of our framework, showcasing its ability to generalize well across multiple tasks even under the scarcity of extensively annotated datasets, offering a scalable solution to automatic segmentation and annotation challenges in the field. In addition, the proposed pipeline is flexible and can be applied to medical image segmentation, remarkably boosting the performance. Note that ALPS utilizes pre-trained SAM to semi-automatically annotate RS images without additional manual annotations. Though every component in the pipeline has been well explored, integrating clustering algorithms with SAM and novel pseudo-label alignment significantly enhances RS segmentation, as an off-the-shelf tool for pre-training data preparation. Our source code is available at: <https://github.com/StriveZs/ALPS>.

Introduction

Semantic segmentation represents a critical task within computer vision, involving pixel-level classification that plays a pivotal role across various applications. This technique, essential for attributing distinct labels to each pixel, facilitates a comprehensive understanding of spatial relationships within images. It stands as a cornerstone in applications ranging from lane detection in autonomous driving (Fischer et al. 2018) to UAV geolocalization efforts (Nassar et al. 2018). Distinguished from image prediction, semantic segmentation delivers an in-depth object delineation, integrating valuable spatial context. This technique has been widely

^{*}These authors contributed equally.

[†]Corresponding author

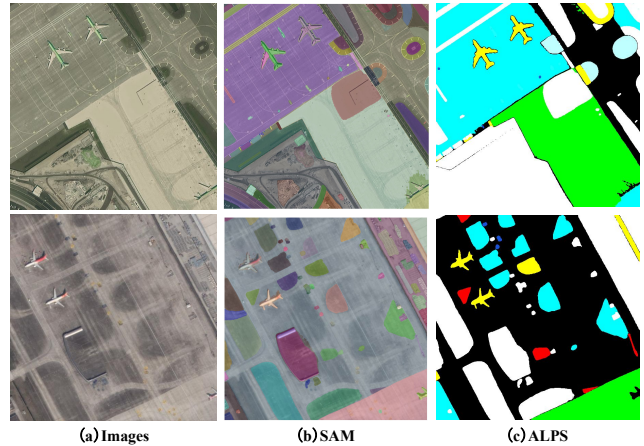


Figure 1: Some examples of SAM segmentation results and ALPS segmentation results on remote sensing images. (a) some remote sensing images obtained from the SAMRS (Wang et al. 2024), (b) segmentation results predicted by the SAM (Kirillov et al. 2023) without any prompts, (c) semantic segmentation results generated by our ALPS without any prompts.

used in multiple areas, especially in addressing complex, data-intensive challenges inherent in remote sensing (RS) (Ball, Anderson, and Chan 2017). In the RS domain, the applications of semantic segmentation span environmental surveillance (Blaschke et al. 2000; Yuan and Sarma 2010), agricultural crop cover and variety determination (Yang et al. 2016; Kussul et al. 2017; Jadhav and Singh 2018), forestry for species recognition (Dechesne et al. 2017), to urban planning through building classification and land-use analysis (Rottensteiner et al. 2012; Volpi and Ferrari 2015; Fang et al. 2018).

The advancement of earth observation technologies has led to the generation of abundant RS images. Yet, annotating these images with precise, pixel-level semantic labels remains laborious and expensive, making the acquisition of extensively annotated datasets for downstream supervised segmentation tasks challenging. In response, researchers have turned to weakly-supervised techniques that employ minimal forms of supervision, such as scribbles

(Lin et al. 2016; Tang et al. 2018a,b; Vernaza and Chandraker 2017; Xu, Schwing, and Urtasun 2015a), bounding boxes (Dai, He, and Sun 2015; Khoreva et al. 2017; Papandreou et al. 2015; Xu, Schwing, and Urtasun 2015b), clicks (Bearman et al. 2016), and image-level tags (Papandreou et al. 2015; Tang et al. 2018b; Xu, Schwing, and Urtasun 2015b), or semi-supervised methods that label only a subset of the dataset (Dai, He, and Sun 2015; Papandreou et al. 2015; Hong, Noh, and Han 2015; Hou et al. 2017; Pathak, Krahenbuhl, and Darrell 2015), both strategies significantly reducing the need for exhaustive human annotation. Despite advancements, the crux of semantic segmentation research still necessitates some degree of manual labeling for training neural networks. Consequently, a new wave of weakly semantic segmentation approaches has emerged, eschewing labels altogether. These pioneering methods harness pixel-level self-supervised representation learning, introducing techniques such as cross-view consistency (Cho et al. 2021; Ji, Henriques, and Vedaldi 2019), edge detection (Hwang et al. 2019; Zhang and Maire 2020), and saliency prior (Van Gansbeke et al. 2021) to autonomously parse and understand RS imagery.

On the other hand, the Segment Anything Model (SAM) (Kirillov et al. 2023) has emerged as a groundbreaking advancement in computer vision, primarily for its outstanding ability in object segmentation. The robust generalization capability enables SAM to exhibit exceptional zero-shot segmentation, even in specialized domains like remote sensing (RS) images (Cheng, Han, and Lu 2017; Camps-Valls et al. 2011; Tuia et al. 2009) and medical imagery (Castellano et al. 2004; Pluim, Maintz, and Viergever 2003; He et al. 2023), leveraging training from a comprehensive natural image dataset. Extensions of SAM, such as SAMFeat (Wu et al. 2023), SA3D (Cen et al. 2024), and SAM-Track (Cheng et al. 2023b), further amplify its utility in tasks ranging from local feature learning to 3D segmentation and video object tracking. Uniquely, in the RS domain, SAM showcases profound zero-shot segmentation potential. Studies like Ren (Ren et al. 2024) and Julka (Julka and Granitzer 2023) have validated SAM’s versatility across different datasets and applications, including planetary geography. New methods like Text2Seg (Zhang et al. 2023) and RSPrompter (Chen et al. 2024) have extended the applications of SAM with text-based guidance and novel prompt learning methods for improved semantic segmentation and instance segmentation, respectively. Moreover, leveraging SAM for data annotation has been explored, with SAMRS (Wang et al. 2024) demonstrating its efficacy in generating large-scale, accurately labeled datasets, showcasing its efficiency and effectiveness of data annotation across computer vision tasks.

However, leveraging SAM to automatically annotate RS images for semantic segmentation presents significant challenges:

- *Detection Annotations and Additional Prompts:* Existing solutions based on SAM, such as SAMRS (Wang et al. 2024), usually need the annotations of object detection or external prompts for semantic label predictions from RS images. However, the objective of our work is to bypass these constraints, enabling SAM to autonomously

generate labels across diverse RS scenarios without external prompts.

- *Random Color Label Assignments by SAM:* When used without any prompts, SAM segments all elements within an image and assigns random color labels. These color labels for objects of the same or different categories lack consistency, rendering them unsuitable for direct use in downstream segmentation training tasks.
- *Inconsistency in Segmentation Results:* The segmentation outcomes for the same image by vanilla SAM can vary. For example, in Figure 1, SAM sometimes identifies the wings and fuselage of a plane as distinct parts, and at other times, considers them as a single entity. This randomness adds another layer of complexity in developing a unified strategy for automatic labeling.

Our study focuses on overcoming these hurdles by formulating a method that allows SAM to allocate unified pixel-level labels to objects of the same category, thereby facilitating an auto-labeling scheme for massive unlabeled data.

To tackle above challenges, this work introduces **ALPS** (Automatic Labeling for Pre-training in Segmentation), a novel auto-labeling framework that leverages the capabilities of the vanilla Segment Anything Model (SAM) for annotating vast quantities of unlabeled remote sensing (RS) images for semantic segmentation. Utilizing the vanilla SAM, we first generate *Unlabeled Instance Mask sets* (UiMs) for each image using the raw output of SAM, then identifying unique segmentation outlines without associated labels. Through an innovative process, high-level features of each mask are extracted to define a *pseudo feature label* (PFL), subsequently clustered via online K-means (Cohen-Addad et al. 2021) to assign a *pseudo class label* (PCL) to each mask. This approach automates the construction of pre-training datasets aimed at enhancing the performance of downstream RS segmentation tasks. Though every component in the proposed pipeline is a well-explored method, their specific applications in conjunction with SAM for RS images and the novel mechanism for aligning pseudo-labels represents a noteworthy adaptation and refinement for RS contexts.

Our technical contributions can be summarized as follows:

- We systematically study the problem of efficiently annotating RS images for segmentation without manual prompts, leveraging a label-level distillation process from SAM. To best of our knowledge, this work is the first to enhance RS pre-training through distilling SAM on unlabeled datasets, by addressing the technical issues including lack of detection annotations, uses of additional prompts, and random & inconsistent outputs of SAM on RS imagery.
- We propose an effective and innovative auto-labeling framework, ALPS, which employs high-level feature clustering to achieve efficient labeling of large-scale datasets using the vanilla SAM. Note that the proposed framework leverages the pre-trained SAM, which is originally trained on human-annotated data. However, in our approach, no additional manual annotations are required

for RS images, thus enabling a semi-automated annotation process without additional human intervention.

- Our extensive experiments on pseudo-labeled pre-training datasets, including iSAID (Waqas Zamir et al. 2019) and SAMRS (Wang et al. 2024), validate our methodology. By conducting segmentation pre-training, our studies underscore the effectiveness of leveraging vast RS segmentation data to mitigate task discrepancies and address the challenges posed by limited training data availability. Experiments show that our ALPS improves mIoU by up to 9.98% compared to SAMRS*.
- The proposed is flexible. We also conduct experiments on medical image segmentation. The experimental results show that the proposed method notably improve the mIoU by at most 6.12%.

This approach has made a significant advancement in utilizing auto-labeled datasets for enhancing the accuracy and efficiency of segmentation models in remote sensing applications.

Preliminaries

In this section, we review the foundation model (SAM) and remote sensing (RS) datasets used in our framework. We primarily employ the vanilla SAM (Kirillov et al. 2023), iSAID dataset (Waqas Zamir et al. 2019) and SAMRS dataset (Wang et al. 2024).

Segment Anything Model

Recently, the SAM (Kirillov et al. 2023), a segmentation model, was recently introduced by Meta AI Research alongside the largest, most comprehensive segmentation dataset to date, SA-1B, containing 1.1 billion masks and 11 million images. Through specially designed training methods and a large-scale training data SA-1B, it offers not only support for interactive segmentation methods but also delivers outstanding zero-shot performance on a wide range of segmentation tasks. These two crucial features significantly enhance the applicability of SAM and make it a promising solution for various computer vision applications. Therefore, in this study, we adopt the vanilla SAM to predict the UiMs and utilize the encoder of vanilla SAM to extract the PFL for each mask.

Datasets For Automatic Labeling

iSAID: iSAID (Waqas Zamir et al. 2019) is a large-scale aerial image segmentation benchmark, which consists of 2,806 high resolution remote sensing (RS) images. These images were collected from multiple sensors and platforms with multiple resolutions. The size of the original images ranges from 800×800 to 4000×13000 . The iSAID dataset provides 655,451 instance annotations over 15 categories, which is one of the largest datasets for instance segmentation in remote sensing. The training set contains 1,411 images, the validation (val) set contains 458 images and the test set has 937 images. In this work, we only use the original images for our ALPS framework.

SAMRS: The SAMRS (Wang et al. 2024) dataset, which stands for Segment Anything Model annotated RS segmentation dataset, is a large-scale segmentation dataset constructed using SAM and off-the-shelf object detection models trained on RS dataset, e.g. HRSC2016 (Liu et al. 2017), DOTA-V2.0 (Ding et al. 2021), DIOR (Li et al. 2020), and FAIR1M-2.0 (Sun et al. 2022). This dataset consists of three subsets: SOTA, SIOR, and FAST. SOTA and SIOR are segmentation datasets containing common object categories, while FAST is a dataset specifically targeting diverse vehicles and grounds. The training set contains 8,685 images, and validation (val) set contains 4,667 images. In this study, we only use the original images for our ALPS framework.

Methodology

This section presents the methodology of ALPS (Automatic Labeling for Pre-training in Segmentation).

Pipeline

Our ALPS framework is in light of achieving unsupervised automatic labeling on massive RS unlabeled data, meanwhile, the data with pseudo labels can be used to pre-train segmentation models to improve the performance of the downstream segmentation tasks. To achieve this goal, we introduce ALPS, an innovative auto-labeling framework based on the vanilla SAM, which comprises two parts – Binary Mask Prediction and Mask Class Association. We first use SAM to obtain the binary masks of instances and then employ a clustering approach to assign a label to each mask. There three steps to achieve the smantic labels. Firstly, we obtain the *pseudo feature label* (PFL) by extracting the regional feature of each mask. Secondly, we apply online K-means for clustering and finally, we assign a *pseudo class label* (PCL) to each mask based on the clustering centers. Fig 2 illustrates the architecture of our ALPS framework.

Specifically, assume there is a large amount of unlabeled RS images $\{I_i\}_{i=0}^N$, given an input image I_i , our ALPS framework firstly uses the vanilla SAM without any additional prompts to obtain the *Unlabeled Instance Mask set* (UiMs) v , then we introduce a binary mask decomposition module to obtain the binary mask of each instance and design a filtering gate to filter out the abnormal masks to alleviate the erosion of the reliable pseudo-labels by the overly large background.

Furthermore, to assign the appropriate label to each mask, we employ the encoder of vanilla SAM (Kirillov et al. 2023) to extract the semantic features F_i from the input image. Subsequently, these features are upsampled to match the scale of the binary mask, thereby facilitating feature alignment. Then we obtain the binary masks sequentially from the set and carry out PFL mapping in conjunction with the aligned feature map. The results of mapping are then fed into an online K-means (Cohen-Addad et al. 2021) to achieve iterative clustering to obtain the PCL for each mask. Finally, by integrating the outputs from the above two parts, we can generate the pseudo-labels through unsupervised automatic labeling for original images. Moreover, benefiting from the generalization of SAM and scalability of K-means,

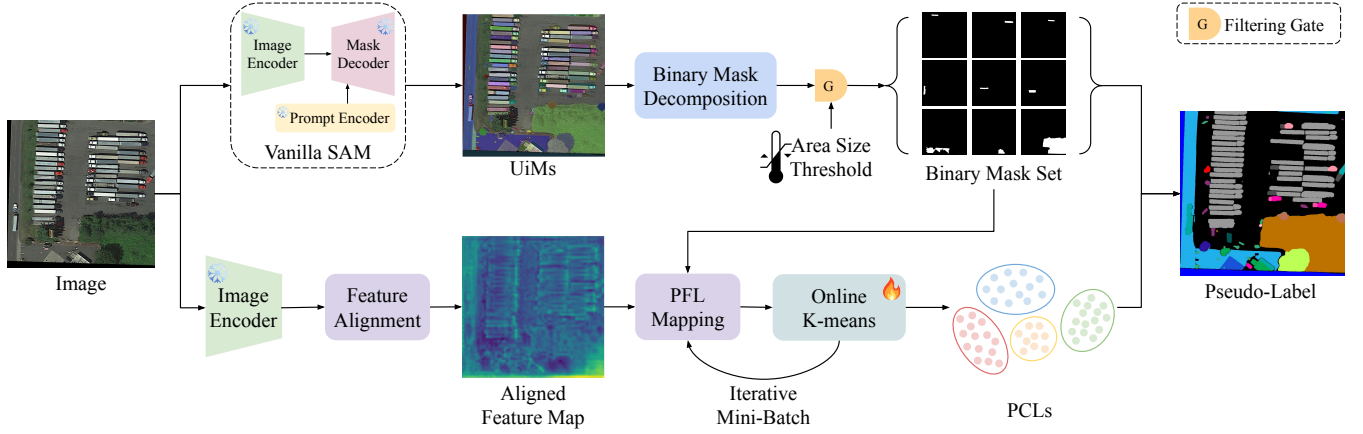


Figure 2: The illustration of our ALPS framework. Our mainly framework consists of two parts, which can obtain the binary mask set and PCL for each mask respectively.

our ALPS framework can easily apply to any similar domain data.

Binary Mask Prediction

UiMs Prediction: In our ALPS framework, we employ the officially provided, pre-trained ViT-H (Dosovitskiy et al. 2020) based SAM model as the toolkit for UiMs prediction. We have leveraged the mechanism of automatic mask generation of vanilla SAM. Specific ally, we take an RS image I_i and default a set of dense prompts \mathcal{P} as input, where the dense prompts are the default configuration of SAM, and outputs the corresponding UiMs in the form of a bitmap, the formulation is defined as Eq. 1:

$$\text{UiMs} = S(I_i, \mathcal{P}) \quad (1)$$

where $S(\cdot)$ represents the inference phase of vanilla SAM.

Binary Mask Generation: After obtain the UiMs, we design a binary mask decomposition module and filtering gate to generate the binary mask set for later process. Specifically, we have developed a module to individually extract each mask from UiMs and convert it into a binary mask for separate storage, by leveraging the characteristic that each mask M in UiMs has color differences in RGB values. Then, to alleviate the erosion of the instance mask by the overly large background mask, we designed a filtering gate $G(\cdot)$ to filter out the overly large background mask. First, we defined a instance proportion $\mathcal{PI}(\cdot)$, which is obtained by calculating the percentage of pixels occupied by the instance in the overall mask, defined as Eq. 2:

$$\mathcal{PI}(M_i) = \frac{\text{num}(p_i^0)}{\text{num}(p_i^0 + p_i^{255})} \quad (2)$$

where $\text{num}(\cdot)$ represents the number of pixels, p_i^0 represents the pixels occupied by the instance, where the RGB value of the instance in the binary mask is $(0, 0, 0)$, and p_i^{255} represents the pixel occupied by the background. Then we use an area size threshold σ (default is 0.3) to filter out binary

masks with too large instance proportions, thereby implementing the mechanism of the filtering gate $G(\cdot)$, defined as Eq. 3:

$$G(M_i) = \begin{cases} M_i & \text{if } \mathcal{PI}(M_i) \leq \sigma \\ - & \text{if } \mathcal{PI}(M_i) > \sigma \end{cases} \quad (3)$$

where “-” indicates that this binary mask is discarded.

Mask Class Association

Feature Extraction and Alignment: After filtering, the binary mask lacks inherent class information, making direct categorization a challenging task. Currently, in both machine learning and deep learning paradigms, features play a pivotal role by providing essential semantic information that facilitates the execution of downstream tasks (Yu et al. 2018; Li et al. 2019; Zhang et al. 2018). Consequently, we propose to extract the semantic features corresponding to each binary mask, which could potentially enhance the accuracy of mask class association. Specifically, to ensure methodological consistency, we employ the image encoder component of the vanilla SAM for the extraction of semantic features from the image. Given an arbitrary resolution RS image I_i , we firstly rescale it into the 1024×1024 resolution to fit the input requirement of the image encoder (ViT-H (Dosovitskiy et al. 2020)), and the feature map $F_i \in \mathbb{R}^{256 \times 64 \times 64}$ is extracted by the ViT-H. Then we design a feature alignment module to upsample the feature map by bilinear interpolation, thereby aligning it with the dimensions of the binary mask $M_i \in \mathbb{R}^{1 \times 256 \times 256}$.

Feature Clustering: Based on the aligned feature map $\hat{F}_i \in \mathbb{R}^{256 \times 256 \times 256}$, we propose a PFL mapping module, which uses the binary mask $M_i \in \mathbb{R}^{1 \times 256 \times 256}$ to execute the conjunction with the aligned feature map \hat{F}_i to obtain the PFL \mathcal{L}_i for each binary mask, defined as Eq. 4:

$$\mathcal{L}_i = \hat{F}_i \odot M_i \quad (4)$$

where \odot represents the element-wise product. Based on the aforementioned process, we can obtain the PFL associated

with each binary mask, i.e., construct a PFL set $\{\mathcal{L}_i\}_{i=0}^N$. However, given the substantial volume of data, often in the order of hundreds of thousands or even millions of images, the direct application of conventional clustering algorithms (Xu and Wunsch 2005; Cao, Zhao, and Wang 2023) may result in complications such as I/O crashes and memory overflow. To resolve this issue, we adopt a learnable online K-means (Cohen-Addad et al. 2021) to split the images into mini-batches to iteratively cluster the PFLs into \mathcal{N} clusters, where \mathcal{N} is set for different datasets, e.g., iSAID: $\mathcal{N} = 16$, SAMRS: $\mathcal{N} = 64$. After completing the feature clustering, we can use the trained clustering model to classify each PCL based on the clustering centers and thus obtain the class of each binary mask. This allows us to predict the classes of all binary masks in the binary mask set, ultimately obtaining the pseudo-label of the image. Moreover, we also provide a scheme for predicting the number of clusters for large-scale datasets without prior knowledge. Specifically, DeepDPM (Ronen, Finder, and Freifeld 2022) can offer an elegant, data-adaptive, and mathematically-principled solution for clustering when \mathcal{N} is unknown. Thus, it can be easily incorporated in our ALPS framework that rely on clustering.

Please be advised that while k-means clustering is a well-explored method, its specific application in conjunction with SAM for RS images and the novel mechanism for aligning pseudo-labels represents a noteworthy adaptation and refinement for RS contexts.

Pseudo-Labeled RS Datasets

This section presents the pseudo-labeled datasets generated by the proposed pipeline for RS pre-training.

iSAID-PL

For the partition of the iSAID-PL dataset, we follow the original iSAID (Waqas Zamir et al. 2019), i.e., 1411 training images, 458 validating images, and 937 testing images. The size of the images remains consistent with the original size. Based on the above original images, we use mmsegmentation (Contributors 2020) to crop the image, generating 33,978 training image patches, 11,644 validating image patches, and 937 testing image patches. For pseudo-labels, we adjust the pixels of the area that has not been covered to 255 by default. We set the number of classes \mathcal{N} to 16 to align with iSAID, and the pixel color corresponding to each category is also one-to-one. Moreover, in order to have a more intuitive understanding of our iSAID-PL, we have visualized some pseudo-labels. As shown in Fig 3a, we can discern that our methodology is capable of efficaciously annotating the majority of planes as green, ships as dark green, freighters as light blue, vehicles as pink, trucks as gray, and houses as dark blue. This superior visualization can be attributed to our feature clustering predicated on PFLs, which facilitates the allocation of identical classes across disparate RS images.

SAMRS-PL

Different from the partition of the SAMRS, we merge the Fast, SIOR, and SOTA datasets into a single comprehensive dataset for processing. This dataset comprises a total

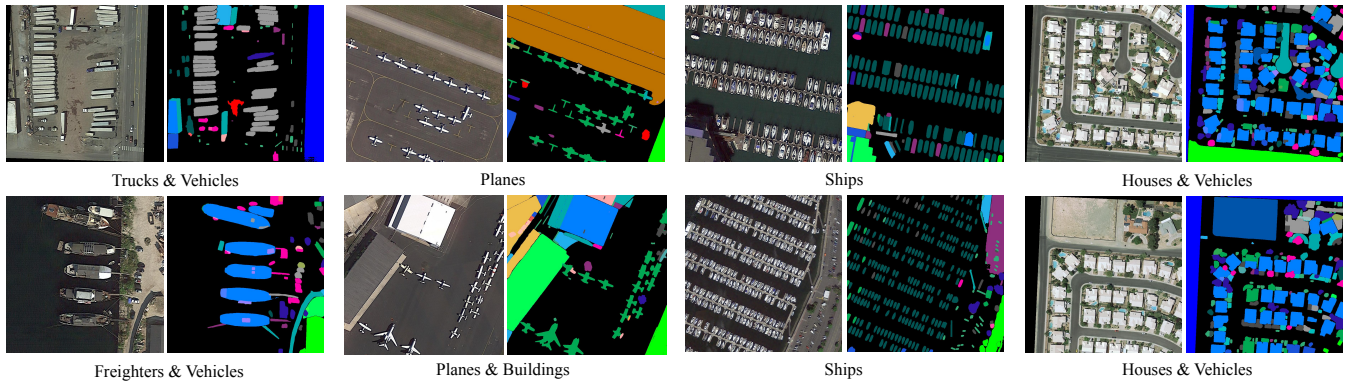
of 105,086 images. We employ a 7:3 ratio to partition the dataset, resulting in 73,560 images for training and 31,526 images for validation. Given that our methodology solely utilizes SAMRS-PL for pre-training, we do not allocate a separate test set. We utilize the ALPS to predict the pseudo-label for each image. For pseudo-label annotations, we adjust the pixels of the area that has not been covered to 255 by default. We set the classes of label \mathcal{N} to 64 to align with SAMRS, and the pixel color corresponding to each category is also one-to-one. As shown in Fig 3b, we have undertaken the visualization of pseudo-labels derived from the SAMRS-PL to foster a deeper comprehension of our methodology. We can observe that our method can effectively annotating the majority of freighters as indigo, ships as pink, planes as light blue and small vehicles as dark blue. Since we have set the \mathcal{N} to 46, which causes the similar color masks within different classes, but these colors is similar but different. The significant visualization can be attributed to our feature clustering predicated on PFLs, which streamlines the assignment of identical classes across different RS images. Nonetheless, it is observable that certain classes may exhibit multiple colors. This could potentially be attributed to an excessively large configuration of the parameter \mathcal{N} , and due to the inherent category differences between instances such as different ships, which subsequently engender disparities among high-level semantic features. However, as can be seen from the aforementioned figure, the annotations predominantly adhere to these colors, with no additional colors being introduced.

Experiment

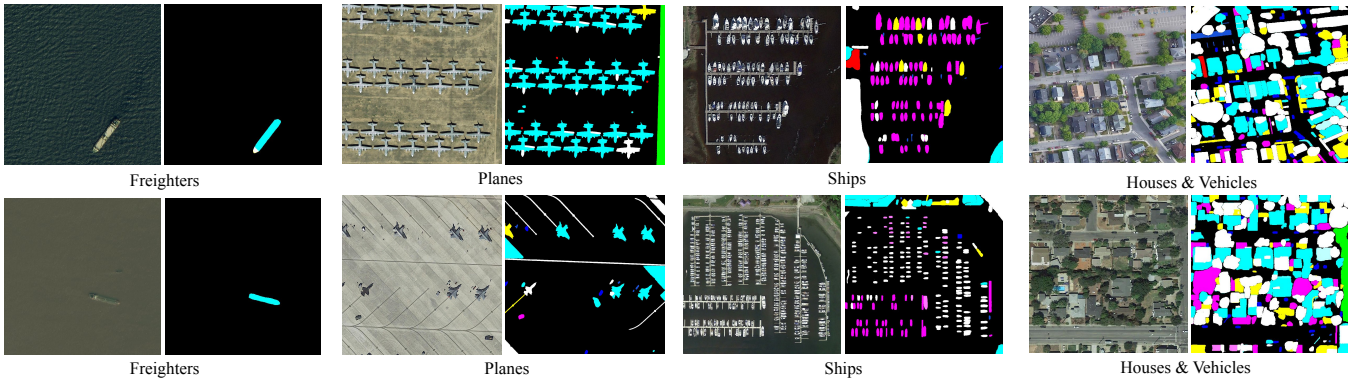
To evaluate the effectiveness of our generated pseudo-labeled RS datasets, we have utilized these datasets for pre-training. The performance of the pre-trained models are then validated across various datasets, e.g., iSAID (Waqas Zamir et al. 2019), ISPRS Potsdam ([Online].).

Experimental Settings

We use the mmsegmentation (Contributors 2020) framework and currently, eight mainstream methods are used as the baseline for pre-training and fine-tuning, e.g., UperNet (Xiao et al. 2018), PspNet (Zhao et al. 2017), HRNet (Wang et al. 2020), Deeplabv3plus (Chen et al. 2018), ViT (Dosovitskiy et al. 2020), Swin-Transformer (Liu et al. 2021), SegMenter (Strudel et al. 2021), SegFormer (Xie et al. 2021). The initial phase of pre-training is executed on the iSAID-PL and SAMRS-PL datasets respectively. Subsequently, fine-tuning is performed on the iSAID and ISPRS Potsdam datasets. This comprehensive process serves to verify the effectiveness of our constructed datasets. Specifically, the specific types of models we use are as follows: UperNet-r50, PspNet-r50, FCN-HRNet-r48, Deeplabv3plus-r50b, ViT-B, Swin-Base, Segmenter-ViT-B, Segformer-MiT-B5. Moreover, in the RS community, iSAID and ISPRS Potsdam have been widely used annotated datasets for evaluating segmentation methods, and we use them to assess the pre-trained models. All experiments are conducted using the PyTorch framework on a setup with 2x NVIDIA GeForce RTX 4090 GPUs under fair configurations.



(a) Some examples of Pseudo-Labels on iSAID-PL dataset.



(b) Some examples of Pseudo-Labels on SAMRS-PL dataset.

Figure 3: Since we have used many types of colors from CoCo (Lin et al. 2014), there may be very similar colors, but the classes they each represent are different. Moreover, these pseudo-labeled RS datasets adopt different random color sets.

Benchmarking on iSAID Dataset

In this section, we have compared the aforementioned methods on iSAID dataset to validate the effectiveness of our pre-training scheme, where are pre-trained on our proposed pseudo-labeled RS datasets. To provide more comprehensive quantitative results, we have divided our pre-trained model into three pre-trained sub-models: overall, backbone, and head. During the fine-tuning phase, we loaded the aforementioned sub-models as initial parameters and then trained them under the same environment and configuration to compare the results with the corresponding baselines. All of the baselines are fine-tuned with the official pre-trained backbones loaded by mmsegmentation. The quantitative results are shown in Table 1, we can observe that following pre-training on pseudo-labeled RS datasets, the fine-tuning results on iSAID surpass the baseline results, e.g., iSAID-PL & Overall: UperNet: 64.90 vs. 64.52, Segformer: 64.89 vs. 64.60, underscoring the efficacy of our predicted pseudo-labels in positively improving the initialization of parameters. We attribute the significant improvement to the integration of segmentation pre-training with pseudo-labels, which provides a valuable prior for segmentation. However, the sub-model of the backbone exhibits relatively weaker performance compared to others. We believe this is due to in-

sufficient pre-training steps. Therefore, we have further explored using a larger number of pre-training steps to validate our analysis, as discussed in Sec .

Benchmarking on ISPRS Potsdam Dataset

Furthermore, to validate the generalization of our constructed pseudo-labeled RS datasets, we have adopted the ISPRS Potsdam dataset during the fine-tuning phrase to mitigate potential issues such as overfitting or diminished generalizability that may arise due to the utilization of images from the identical domain in both the iSAID and iSAID-PL. The quantitative results are presented in Table 2. Contrary to the fine-tuning results on iSAID, the performance of each method on the ISPRS Potsdam dataset is more closely aligned. And we can observe that all of methods demonstrate enhanced performance relative to their respective baselines, e.g., SAMRS-PL & Overall: UperNet: 71.29 vs. 71.18, Segformer: 71.81 vs. 71.50. Moreover, it is noteworthy that in the ISPRS Potsdam dataset, the performance disparity between the backbone sub-model and other sub-models is not substantial like results on iSAID. Based on the evaluation results on iSAID and Potsdam datasets, we can conduct the effectiveness and generalization of our proposed pseudo-labeled RS datasets in downstream tasks, which means the

Methods	Type	Pre-trained	Step	BG	SH	ST	BD	TC	BC	GTF	BR	LV	SV	HC	SP	RA	SBF	PL	HA	mIoU	mAcc
Convolution Based Network																					
UperNet	Baseline	-	80k	98.67	68.80	71.29	71.98	86.67	52.68	57.35	39.94	63.29	48.30	0.00	48.09	47.35	72.38	82.74	58.20	64.52	73.70
	Overall	iSAID-PL	80k	98.61	68.28	72.05	71.74	86.79	52.44	56.58	40.25	63.26	48.56	0.00	54.67	47.29	70.50	82.93	59.58	64.90	73.96
	Backbone	iSAID-PL	80k	98.39	59.85	62.92	61.74	83.12	42.24	52.28	29.92	56.92	45.22	0.00	48.31	46.28	61.27	76.66	53.96	58.61	65.16
	Head	iSAID-PL	80k	98.67	70.20	70.34	76.33	88.18	61.91	56.54	40.37	63.67	49.37	0.00	50.92	58.53	73.83	83.68	57.56	66.67	74.38
	Overall	SAMRS-PL	80k	98.65	67.83	71.23	69.63	87.13	52.65	57.32	40.01	63.20	45.76	0.00	52.58	49.87	73.77	82.38	57.80	64.65	74.17
	Backbone	SAMRS-PL	80k	98.42	58.44	63.38	67.39	84.42	42.98	45.68	29.86	56.85	33.61	0.00	45.76	40.94	65.49	78.43	50.37	57.47	64.68
PspNet	Baseline	-	80k	98.70	70.59	72.46	75.77	88.52	52.30	56.85	41.33	63.29	49.62	0.00	47.28	59.24	73.87	83.87	57.86	66.10	73.51
	Overall	iSAID-PL	80k	98.66	69.03	72.52	73.27	87.93	64.52	56.83	37.98	62.41	45.01	0.00	50.46	55.62	76.01	82.10	54.30	61.67	74.41
	Backbone	iSAID-PL	80k	98.70	69.84	73.16	73.93	88.68	65.50	57.18	41.53	63.08	46.91	0.00	51.93	62.49	76.78	83.30	56.43	63.09	71.56
	Head	iSAID-PL	80k	98.22	57.43	68.45	66.44	72.19	57.33	40.82	36.64	55.13	30.84	0.00	42.57	50.94	66.58	75.91	43.02	53.17	62.74
	Overall	SAMRS-PL	80k	98.64	69.32	72.85	72.13	87.46	62.73	56.63	40.97	62.48	46.56	0.00	51.40	62.00	75.89	82.61	56.61	62.39	71.99
	Backbone	SAMRS-PL	80k	98.61	70.25	74.41	75.10	88.94	65.64	57.22	41.04	67.42	47.14	0.00	54.21	63.20	77.67	88.03	58.73	64.37	75.00
HRNet	Baseline	-	80k	98.15	62.62	70.50	65.47	77.15	57.50	44.79	37.72	58.86	35.51	0.00	41.22	41.70	70.22	76.04	45.22	55.17	68.41
	Overall	iSAID-PL	80k	98.64	68.13	73.27	75.54	87.79	54.28	60.11	42.53	62.39	47.35	0.00	42.34	64.02	75.93	85.16	54.80	62.02	74.05
	Backbone	iSAID-PL	80k	98.71	68.80	67.55	74.43	87.82	58.66	55.16	42.36	60.03	50.24	0.00	48.57	62.93	77.74	84.30	59.37	62.54	73.82
	Head	iSAID-PL	80k	98.66	69.13	67.65	74.03	87.53	61.68	59.78	44.96	62.60	49.11	0.00	47.39	61.11	73.25	83.02	60.15	62.50	72.18
	Overall	SAMRS-PL	80k	98.41	58.12	54.29	60.49	82.88	42.54	43.50	32.65	54.93	45.95	0.00	43.12	56.36	66.94	78.27	59.89	54.27	59.30
	Backbone	SAMRS-PL	80k	98.71	69.41	72.14	75.69	87.67	61.36	58.07	41.33	62.91	49.58	0.00	47.81	69.01	78.20	83.92	59.73	63.47	74.50
Deeplabv3plus	Baseline	-	80k	98.66	69.13	67.65	74.03	87.53	61.68	59.78	44.96	62.60	49.11	0.00	47.39	65.11	73.25	83.02	60.15	62.75	73.32
	Overall	iSAID-PL	80k	98.41	58.39	56.16	60.00	82.66	46.82	43.44	32.73	54.58	45.52	0.00	47.07	60.12	76.16	78.00	60.28	55.27	62.10
	Backbone	iSAID-PL	80k	98.70	67.77	71.98	74.21	87.87	63.71	59.03	42.51	63.62	51.40	0.00	50.44	67.89	75.21	84.57	58.58	63.59	74.64
	Head	iSAID-PL	80k	98.62	70.07	69.55	58.06	88.33	60.25	56.44	41.11	64.11	47.49	0.00	51.70	42.52	72.34	81.27	58.34	60.01	74.27
	Overall	SAMRS-PL	80k	98.62	66.61	71.80	66.93	87.06	59.82	57.65	36.52	62.61	46.79	0.00	57.22	47.14	70.89	80.18	57.68	60.46	73.94
	Backbone	SAMRS-PL	80k	98.23	54.05	54.80	53.80	78.72	46.86	55.82	28.72	52.70	42.02	0.00	49.30	36.60	55.04	74.81	47.77	51.79	59.39
Transformer Based Network																					
ViT	Baseline	-	160k	98.62	66.81	68.87	77.13	85.33	56.27	63.17	46.87	59.27	38.91	0.00	47.24	67.58	73.80	80.05	52.79	61.42	72.51
	Overall	iSAID-PL	160k	98.64	66.31	68.94	75.68	85.75	57.55	63.80	43.80	60.48	39.52	0.00	46.55	67.63	75.83	80.46	52.74	61.48	72.57
	Backbone	iSAID-PL	160k	98.63	66.17	69.19	75.43	85.51	57.53	60.88	38.59	60.42	39.76	0.00	48.24	67.80	74.01	80.19	52.66	60.94	72.43
	Head	iSAID-PL	160k	98.64	67.15	68.61	78.08	85.53	55.67	61.87	45.93	60.42	39.58	0.00	51.04	70.76	74.19	80.26	55.27	62.06	72.90
	Overall	SAMRS-PL	160k	98.63	66.66	69.11	76.44	84.49	60.41	59.47	45.26	60.01	38.48	0.00	49.97	67.11	73.84	80.38	55.71	61.62	72.41
	Backbone	SAMRS-PL	160k	98.63	66.74	69.11	77.42	85.51	57.70	60.63	42.68	60.34	38.78	0.00	47.94	65.88	74.36	80.14	53.64	61.22	72.16
Swin	Baseline	-	160k	98.62	66.14	68.75	78.30	85.86	56.79	61.52	46.89	58.68	39.63	0.00	47.44	68.31	73.97	79.89	54.04	61.55	72.83
	Overall	iSAID-PL	160k	98.74	71.25	73.93	80.11	88.61	61.76	60.36	39.38	64.27	48.93	0.00	49.32	66.71	77.30	84.32	59.03	64.00	75.30
	Backbone	iSAID-PL	160k	98.75	71.17	73.62	81.76	88.76	63.00	60.29	39.48	64.71	49.39	0.00	49.52	66.59	76.34	84.43	60.23	64.25	75.10
	Head	iSAID-PL	160k	98.74	73.40	72.38	78.91	88.35	62.62	59.93	44.49	64.57	48.97	0.00	50.56	68.59	76.41	84.30	58.99	64.45	75.20
	Overall	SAMRS-PL	160k	98.75	72.08	74.14	78.32	88.56	64.15	60.49	46.18	64.65	49.51	0.00	51.14	67.72	77.01	84.43	58.88	64.75	75.40
	Backbone	SAMRS-PL	160k	98.76	73.16	72.77	80.39	88.64	63.83	64.44	41.58	64.81	48.82	0.00	51.27	66.32	77.08	84.34	60.97	64.82	76.12
Segmenter	Baseline	-	160k	98.75	71.36	72.29	79.26	88.31	64.56	62.64	43.77	65.10	48.82	0.00	51.54	69.04	76.57	84.48	60.15	64.79	75.75
	Overall	iSAID-PL	160k	98.76	72.79	72.99	79.93	89.27	62.51	62.06	44.15	64.70	49.20	0.00	50.49	67.18	77.66	84.51	58.13	64.75	75.59
	Backbone	iSAID-PL	160k	98.30	56.36	58.47	72.03	79.94	56.20	62.86	35.64	48.59	23.13	0.00	35.45	60.65	76.24	65.70	39.38	57.93	66.20
	Head	iSAID-PL	160k	98.32	56.11	59.44	74.14	80.98	54.04	62.71	33.56	49.43	23.10	0.00	35.47	59.58	76.53	66.74	39.12	57.95	66.17
	Overall	SAMRS-PL	160k	98.31	55.23	59.19	75.53	81.11	54.41	61.75	32.43	50.09	22.86	0.00	27.51	60.92	74.60	66.77	38.69	57.29	65.92
	Backbone	SAMRS-PL	160k	98.32	55.98	58.56	74.65	80.19	54.80	61.79	33.21	50.24	23.32	0.00	32.27	65.85	75.51	66.38	41.44	58.17	66.37
Segformer	Baseline	-	160k	98.29	55.38	58.03	75.15	81.22	55.81	61.69	33.10	50.79	22.89	0.00	28.02	61.33	74.17	66.43	38.32	57.37	66.28
	Overall	iSAID-PL	160k	98.30	55.64	58.59	74.50	79.98	57.09	62.83	38.09	49.15	21.60	0.00	33.81	60.27	75.69	65.63	40.37	58.10	66.36
	Backbone	iSAID-PL	160k	98.73	70.99	74.07	79.18	88.53	64.12	66.01	43.82	64.23	46.15	0.00	47.12	71.58	77.48	83.55	58.09	64.60	75.62
	Head	iSAID-PL	160k	98.75	72.05	73.49	79.33	88.30	66.92	65.58	41.90	64.41	46.38	0.00	46.79	75.34	77.52	83.52	57.99	64.89	75.97
	Overall	SAMRS-PL	160k	98.73	70.18	73.17	77.31	88.04	61.73	64.38	46.31	63.12	46.88	0.00	50.12	70.33	78.48	83.27	56.81	64.30	75.34
	Backbone	SAMRS-PL	160k	98.74	70.57	73.39	79.24	88.50	62.05	66.68	44.87	63.57	47.02	0.00	49.76	73.56	78.30	83.70	57.77	64.86	75.86
Segformer	Baseline	-	160k	98.76	72.32	73.57	80.03	89.05	64.76	65.6	46.68	63.05	46.75	0.00	46.98	75.53	78.91	83.67	59.84	65.35	76.53
	Overall	iSAID-PL	160k	98.76	72.67	72.81	80.57	88.14	63.45	65.50	41.55	63.68	46.55	0.00	48.53	72.16	78.78	83.70	58.33	64.70	75.97
	Backbone	iSAID-PL	160k	98.74	71.25	73.82	79.47	88.32	64.87	62.61	45.26	63.31	46.09	0.00	46.82	73.43	79.61	83.63	59.96	64.82	75.60
	Head	iSAID-PL	160k	98.76	72.79	72.99	79.93	89.27	62.51	62.06	44.15	64.70	49.20	0.00	50.49	67.18	77.66	84.51	58.13	64.75	75.59

Methods	Type	Pre-trained	Step	IS	BD	LV	TR	CR	CL	mIoU	mAcc
Convolution Based Network											
UperNet	Baseline	-	80k	81.06	89.02	70.57	74.39	74.17	37.88	71.18	83.74
	Overall	iSAID-PL	80k	80.73	89.84	69.77	73.99	74.67	38.52	71.25	85.07
	Backbone	iSAID-PL	80k	80.62	89.70	70.04	73.78	73.26	37.64	70.84	84.78
	Head	iSAID-PL	80k	81.17	89.98	70.34	74.46	74.18	38.19	71.39	85.33
	Overall	SAMRS-PL	80k	81.08	90.10	70.15	74.47	74.38	37.55	71.29	85.10
	Backbone	SAMRS-PL	80k	80.86	89.58	69.78	74.12	74.10	37.77	71.03	84.95
Pspnet	Baseline	-	80k	81.13	89.80	70.30	74.44	73.88	37.39	71.16	85.15
	Overall	iSAID-PL	80k	80.98	89.78	70.62	74.48	73.72	39.24	71.47	85.39
	Backbone	iSAID-PL	80k	78.02	88.33	69.98	73.75	72.90	36.41	69.89	80.38
	Head	iSAID-PL	80k	81.15	90.13	70.20	74.35	75.10	38.94	71.64	85.46
	Overall	SAMRS-PL	80k	80.94	89.65	70.50	74.47	73.95	38.89	71.40	85.37
	Backbone	SAMRS-PL	80k	79.99	88.61	70.02	73.60	73.83	37.30	70.56	84.57
HRNet	Baseline	-	80k	81.13	90.02	70.07	74.35	74.41	38.76	71.46	85.40
	Overall	iSAID-PL	80k	80.59	89.44	69.74	73.63	72.96	37.41	70.63	84.86
	Backbone	iSAID-PL	80k	80.27	89.33	70.09	73.92	73.87	39.54	71.17	85.25
	Head	iSAID-PL	80k	80.37	88.99	69.47	73.35	73.30	38.11	70.60	84.76
	Overall	SAMRS-PL	80k	80.95	89.96	70.70	74.74	73.93	37.62	71.30	85.12
	Backbone	SAMRS-PL	80k	80.83	89.98	70.23	74.63	73.94	36.19	70.97	85.31
DeepLabv3plus	Baseline	-	80k	81.05	89.97	70.60	74.74	74.29	38.59	71.54	85.27
	Overall	iSAID-PL	80k	80.93	90.17	69.91	74.32	74.77	37.45	71.26	85.02
	Backbone	iSAID-PL	80k	81.07	90.06	70.33	74.25	73.71	39.44	71.48	85.53
	Head	iSAID-PL	80k	81.26	93.35	70.06	74.67	74.26	38.22	71.39	85.30
	Overall	SAMRS-PL	80k	80.86	90.03	70.52	74.32	73.46	39.37	71.43	85.31
	Backbone	SAMRS-PL	80k	80.97	90.07	69.71	73.95	73.76	39.33	71.29	85.05
Transformer Based Network											
ViT	Baseline	-	160k	80.10	89.42	70.39	73.65	73.49	35.52	70.25	84.26
	Overall	iSAID-PL	160k	80.51	89.53	70.48	73.50	73.05	35.88	70.49	84.46
	Backbone	iSAID-PL	160k	80.46	89.20	70.39	73.59	73.09	35.29	70.34	84.32
	Head	iSAID-PL	160k	81.14	89.95	70.30	73.56	73.13	37.05	70.85	84.77
	Overall	SAMRS-PL	160k	80.83	89.66	69.98	73.22	73.24	34.88	70.30	84.24
	Backbone	SAMRS-PL	160k	80.54	89.39	70.28	73.55	73.25	35.21	70.37	84.34
Swin	Baseline	-	160k	81.34	89.73	70.29	73.55	72.85	36.96	70.79	84.77
	Overall	iSAID-PL	160k	81.21	90.03	71.04	74.72	73.64	37.11	71.29	85.11
	Backbone	iSAID-PL	160k	81.71	90.22	71.15	74.77	73.94	39.78	71.93	85.61
	Head	iSAID-PL	160k	81.15	90.01	70.96	74.70	73.65	38.21	71.45	85.33
	Overall	SAMRS-PL	160k	81.50	90.30	70.93	74.92	73.90	37.82	71.56	85.30
	Backbone	SAMRS-PL	160k	81.34	90.23	70.86	74.73	73.55	37.7	71.40	85.21
Segmenter	Baseline	-	160k	81.55	90.31	70.92	74.68	73.93	38.91	71.72	85.49
	Overall	iSAID-PL	160k	81.58	90.27	71.19	74.98	74.27	39.52	72.00	85.68
	Backbone	iSAID-PL	160k	80.94	89.14	70.95	74.28	71.95	37.18	70.74	84.76
	Head	iSAID-PL	160k	80.47	89.99	71.05	74.32	72.39	37.15	70.90	84.60
	Overall	SAMRS-PL	160k	80.72	89.30	70.73	74.29	72.12	36.70	70.64	84.60
	Backbone	SAMRS-PL	160k	80.62	89.77	70.95	74.26	72.33	36.49	70.74	84.54
Segformer	Baseline	-	160k	81.02	89.27	70.72	74.00	71.97	37.68	70.78	84.71
	Overall	iSAID-PL	160k	80.63	89.16	70.80	74.08	71.80	37.62	70.68	84.72
	Backbone	iSAID-PL	160k	80.83	89.57	71.13	74.21	71.91	37.74	70.90	84.83
	Head	iSAID-PL	160k	81.58	90.09	71.41	74.98	73.46	37.48	71.50	84.16
	Overall	SAMRS-PL	160k	81.78	90.48	71.47	75.11	73.83	39.93	72.10	85.72
	Backbone	SAMRS-PL	160k	81.58	89.96	71.36	74.96	73.53	36.80	71.37	84.89
Transformer Based Network											
Segformer	Baseline	-	160k	81.89	90.52	71.62	75.24	73.81	38.52	71.93	84.52
	Overall	iSAID-PL	160k	81.81	90.45	71.13	74.87	73.75	38.86	71.81	85.49
	Backbone	iSAID-PL	160k	81.82	90.36	71.13	74.88	73.51	38.77	71.74	85.52
	Head	iSAID-PL	160k	82.06	90.60	71.55	75.21	73.61	41.12	71.86	85.56
	Overall	SAMRS-PL	160k	81.89	90.52	71.62	75.24	73.81	38.52	71.93	84.52
	Backbone	SAMRS-PL	160k	81.81	90.45	71.13	74.87	73.75	38.86	71.81	85.49

Table 2: Segmentation results of different methods on the ISPRS Potsdam dataset ([Online]). IS: impervious surface. BD: building. LV: low vegetation. TR:tree. CR: car. CL: clutter

Methods	Type	Pre-trained	Step	BG	SH	ST	BD	TC	BC	GTF	BR	LV	SV	HC	SP	RA	SBF	PL	HA	mIoU	mAcc
UperNet	Backbone	SAMRS*	80k	98.22	57.99	58.38	50.35	82.21	41.54	45.67	26.33	52.91	35.23	0.00	31.75	38.87	51.51	76.56	51.95	53.30	63.50
	Backbone	SAMRS-PL	80k	98.42	58.44	63.38	67.39	84.42	42.98	45.68	29.86	56.85	33.61	0.00	45.76	40.94	65.49	78.43	50.37	57.47	64.68
	Overall	SAMRS*	80k	98.35	58.91	63.59	54.82	81.15	46.19	49.68	32.04	59.83	41.51	0.00	52.23	42.45	69.14	75.62	56.17	58.78	67.67
	Overall	SAMRS-PL	80k	98.65	67.83	71.23	69.63	87.13	52.65	57.32	40.01	63.20	45.76	0.00	52.58	49.87	73.77	82.38	57.80	64.65	74.17
Segformer	Backbone	SAMRS*	160k	98.73	70.31	73.40	79.52	88.01	63.13	63.73	47.40	63.47	46.03	0.00	47.82	65.59	76.93	83.53	59.40	64.19	75.04
	Backbone	SAMRS-PL	160k	98.76	72.67	72.81	80.57	88.14	63.45	65.50	41.55	63.68	46.55	0.00	48.53	72.16	78.78	83.70	58.33	64.70	75.97
	Overall	SAMRS*	160k	98.73	70.79	72.95	79.91	88.00	64.28	66.32	48.11	63.83	46.94	0.00	50.10	66.12	77.93	83.62	59.07	64.80	75.75
	Overall	SAMRS-PL	160k	98.76	72.32	73.57	80.03	89.05	64.76	65.6	46.68	63.05	46.75	0.00	46.98	75.53	78.91	83.67	59.84	65.35	76.53
UperNet	Backbone	Binary Mask	80k	96.98	25.20	0.00	0.00	0.00	0.00	0.00	0.00	19.82	0.12	0.00	0.00	0.00	0.00	0.23	17.81	11.03	11.97
	Backbone	iSAID-PL	80k	98.39	59.85	62.92	61.74	83.12	42.24	52.28	29.92	56.92	45.22	0.00	48.31	46.28	61.27	76.66	53.96	58.61	65.16
	Backbone	SAMRS-PL	80k	98.42	58.44	63.38	67.39	84.42	42.98	45.68	29.86	56.85	33.61	0.00	45.76	40.94	65.49	78.43	50.37	57.47	64.68
	Backbone	Mixed-PL	80k	98.08	59.33	67.74	67.85	87.00	53.64	60.64	52.13	59.82	47.69	0.00	50.05	49.14	68.48	78.86	54.39	59.68	68.33
Segformer	Backbone	Binary Mask	160k	97.10	30.30	0.88	0.00	0.00	0.00	0.00	0.00	21.98	3.21	0.00	0.00	0.00	0.00	2.79	19.88	11.01	13.55
	Backbone	iSAID-PL	160k	98.73	70.18	73.17	77.31	88.04	61.73	64.38	46.31	63.12	46.88	0.00	50.12	70.33	78.48	83.27	56.81	64.30	75.34
	Backbone	SAMRS*	160k	98.76	72.67	72.81	80.57	88.14	63.45	65.50	41.55	63.68	46.55	0.00	48.53	72.16	78.78	83.70	58.33	64.70	75.97
	Backbone	Mixed-PL	160k	98.74	71.35	72.21	81.78	88.41	60.48	66.30	47.64	62.95	46.19	0.00	49.53	72.60	77.71	83.22	59.53	64.91	76.04

Table 3: (a) Quantitative results of different pre-training datasets constructed by different unsupervised manners. SAMRS* represent the data generated by Oriented RepPoints & SAMRS framework. (b) Quantitative results of different pre-trained schemes on the iSAID dataset.

4a, and we can observe that limited by the generalization of the detection model, the segmentation results obtained by SAMRS* actually get worse than ours in some ships and planes images. Benefiting from feature clustering in our mask class association, our method can generate segmentation maps with better visual effects without additional super-vision information.

Please be advised that although the individual performance improvements might appear marginal, the cumulative effect across varying RS segmentation tasks highlights the robustness and generalized enhancement provided by ALPS.

Ablation Study

Effectiveness of Mask Class Association: To verify the effectiveness of our proposed mask class association, we

constructed a comparative baseline solely implemented by the binary mask prediction (Sec). Since the UiMs predicted by vanilla SAM do not correspond to specific target classes, it is reasonable to consider assigning these UiMs as a unified class to obtain the binary masks. Therefore, as shown in Fig 4b, we have generated a set of binary masks for the iSAID dataset and then pre-training using UperNet, comparing the results with UperNet pre-training on our iSAID-PL. The quantitative results are shown in Table 3b, we can discern a substantial disparity between the method pre-training on the binary masks and the methods pre-training on our generated datasets, denoted by a notable difference in performance metrics, e.g., UperNet: mIoU: 10.01 vs. 58.61 vs. 57.47, Segformer: mIoU: 11.03 vs. 64.30 vs. 64.70. Specifically, in the process of the binary mask prediction, we ag-

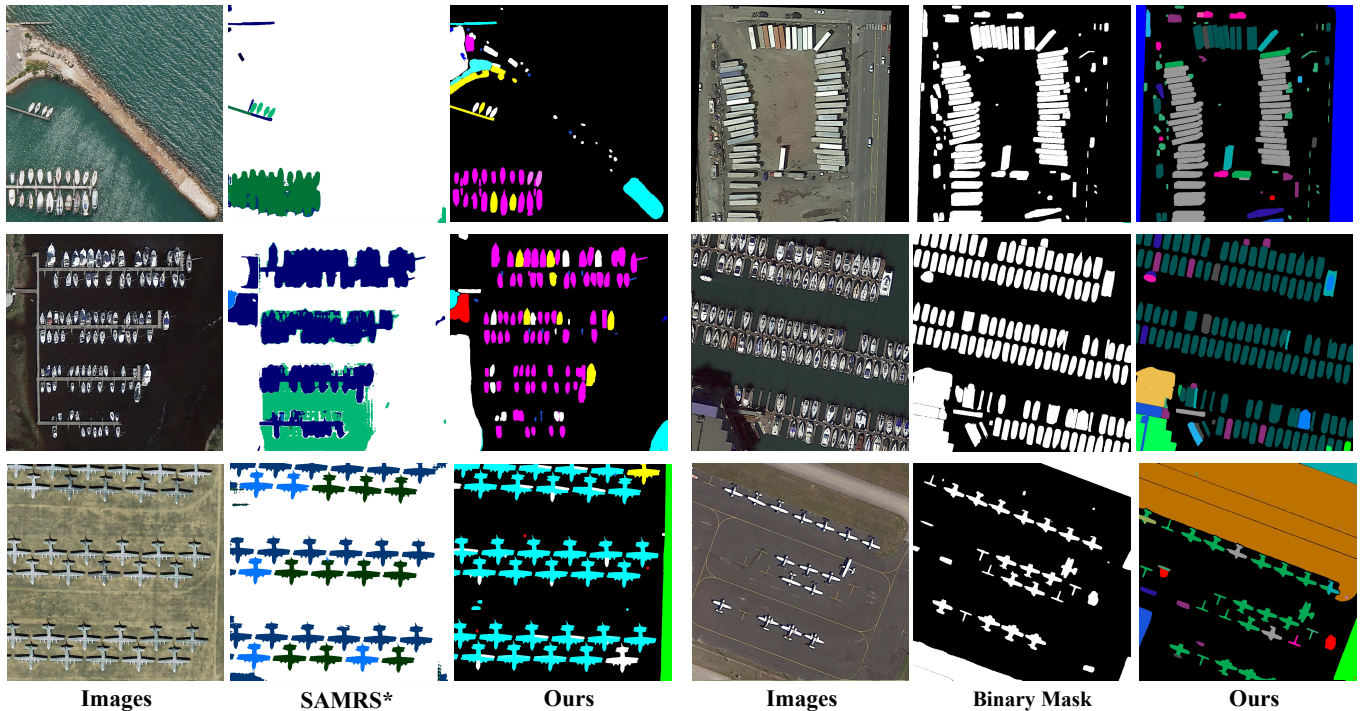


Figure 4: (a) Qualitative results of different pre-training datasets constructed by different unsupervised manners. (b) Some examples of binary masks generated by vanilla SAM.

gregate the binary mask set filtered through the filtering gate $G(\cdot)$ by stacking, thus forming a complete binary mask. To prevent large background masks from overshadowing instances, we set a relatively large area size threshold to filter out larger masks, retaining only smaller instances as foreground, which causes the pre-trained method demonstrates segmentation performance solely on the background, vehicle, plane and harbor. Nevertheless, benefiting from the feature clustering of our mask class association, ALPS can effectively avoid the above issues and generate pseudo-labels that can be used for pre-training to improve the performance of downstream tasks.

Effectiveness of Larger Pre-training data: To validate the larger pre-training data can improve the performance of fine-tuning, we have utilized the iSAID-PL & SAMRS-PL into a Mixed-PL pre-training manner. Specifically, since the inconsistent number of categories in the two datasets, cannot be directly used for mixed training, we considerably load the backbone weight obtained from the iSAID-PL to pre-train on the SAMRS-PL, with either 80k or 160k steps. As shown in Table 3b, using the larger pre-trained data can effectively enhance the performance of UperNet and Segformer on iSAID dataset. We attribute this significant improvement to the data enhancement effect on the model backbone, which is achieved by the richer semantic features brought by an increased number of RS images.

Effectiveness of Larger Pre-training Steps To ensure the potential effectiveness of the pseudo-labels generated

by our ALPS framework, we have pre-trained previous eight methods with larger pre-training steps (e.g. 320k) on our SAMRS-PL dataset and fine-tuned on two validation datasets. The quantitative results are shown in Table. 4. We can observe that the performance improves significantly when larger pre-training steps are employed. This enhanced performance surpasses previous results obtained by 80k or 160k steps when only the backbone weights of the pre-trained model are utilized for fine-tuning. Moreover, after 320k pre-training on SAMRS-PL dataset, a substantial enhancement in performance has been observed for the majority of convolution-based methods. However, the improvement is less pronounced for most transformer-based methods. We attribute this discrepancy is due to the inherent complexity of the self-attention mechanism, which may require a larger number of training steps to converge effectively.

Area Size Threshold Selection During the dataset construction phase, we did not use a filtering gate to filter out overly large background images, which might have caused the SAM to treat all backgrounds other than the foreground target as a whole. However, SAM itself may have certain detection omissions, resulting in inconsistencies such as some targets, like vehicles, being classified as foreground while others are classified as background. This could potentially affect the effectiveness of pre-training. Therefore, we designed a filtering gate to filter out larger masks by a pre-set area size threshold. To select the appropriate area size threshold, we have chosen five different area size thresholds

Methods	Type	Pre-trained	Fine-tuned	Step	mIoU	mAcc
Convolution Based Network						
UperNet	Backbone	SAMRS-PL	iSAID	80k	57.47	64.68
	Backbone	SAMRS-PL	iSAID	320k	61.77	70.95
	Backbone	SAMRS-PL	Potsdam	80k	71.03	84.95
	Backbone	SAMRS-PL	Potsdam	320k	71.31	86.72
Pspnet	Backbone	SAMRS-PL	iSAID	80k	55.17	68.41
	Backbone	SAMRS-PL	iSAID	320k	60.28	70.65
	Backbone	SAMRS-PL	Potsdam	80k	70.56	84.57
	Backbone	SAMRS-PL	Potsdam	320k	71.17	85.15
HRNet	Backbone	SAMRS-PL	iSAID	80k	55.27	62.10
	Backbone	SAMRS-PL	iSAID	320k	59.24	70.88
	Backbone	SAMRS-PL	Potsdam	80k	69.50	84.21
	Backbone	SAMRS-PL	Potsdam	320k	71.05	85.22
DeepLabv3plus	Backbone	SAMRS-PL	iSAID	80k	52.93	60.78
	Backbone	SAMRS-PL	iSAID	320k	58.05	70.61
	Backbone	SAMRS-PL	Potsdam	80k	70.17	84.41
	Backbone	SAMRS-PL	Potsdam	320k	71.09	84.93

Methods	Type	Pre-trained	Fine-tuned	Step	mIoU	mAcc
Transformer Based Network						
ViT	Backbone	SAMRS-PL	iSAID	160k	61.22	72.16
	Backbone	SAMRS-PL	iSAID	320k	61.50	72.44
	Backbone	SAMRS-PL	Potsdam	160k	70.37	84.34
	Backbone	SAMRS-PL	Potsdam	320k	70.53	84.90
Swin	Backbone	SAMRS-PL	iSAID	160k	64.79	75.75
	Backbone	SAMRS-PL	iSAID	320k	64.95	75.97
	Backbone	SAMRS-PL	Potsdam	160k	71.72	85.49
	Backbone	SAMRS-PL	Potsdam	320k	72.19	85.70
Segmenter	Backbone	SAMRS-PL	iSAID	160k	57.37	66.28
	Backbone	SAMRS-PL	iSAID	320k	57.42	66.33
	Backbone	SAMRS-PL	Potsdam	160k	70.68	84.72
	Backbone	SAMRS-PL	Potsdam	320k	70.82	84.74
Segformer	Backbone	SAMRS-PL	iSAID	160k	64.70	75.04
	Backbone	SAMRS-PL	iSAID	320k	64.81	75.76
	Backbone	SAMRS-PL	Potsdam	160k	71.74	85.52
	Backbone	SAMRS-PL	Potsdam	320k	71.86	85.99

Table 4: Quantitative results of larger pre-trained steps on the different datasets.

Area Size Threshold	Backbone	Step	mIoU	mAcc
0.1	UperNet	80K	70.17	83.73
0.3	UperNet	80K	71.03	84.95
0.5	UperNet	80K	65.22	76.90
0.7	UperNet	80K	47.81	57.00
1.0	UperNet	80K	42.99	54.35

Table 5: The ablation study of different area size thresholds.

of 0.1, 0.3, 0.5, 0.7, and 1.0 to construct the dataset for pre-training and fine-tuning tasks. The results of our fine-tuning on Potsdam dataset are shown in the Table 5:

From the above results, we can observe that when the area size threshold is 0.3, it obtains the best performance. The reason for poorer performance at other area size thresholds is analyzed as follows: 0.1 may filter out some larger main targets, such as large aircraft; 0.5 might retain some large background areas, for instance, SAM sometimes divides roads into sections, which could result in these road backgrounds being retained; 0.7 and 1.0 tend to retain larger backgrounds, thus affecting pre-training performance. Therefore, we selected an area size threshold of 0.3 for data generation in our specific experiments.

Generalization on Medical Domain: an External Validation Study

To further validate the generalization of ALPS on medical domain, we have utilized the ATLAS2023 dataset (Quinton et al. 2023), a resource within the medical segmentation domain, to evaluate the efficacy of our ALPS for unsupervised auto-labeling of medical images. The ATLAS2023 dataset, designed for the automatic segmentation of tumors and livers, comprises T1 CE-MRI liver scans from 90 patients with unresectable liver cancer and 90 corresponding liver and liver tumor segmentation masks. These are divided into training and testing cohorts, consisting of 60 and 30 patients respectively. Given that the CE-MRI images (utilizing a gadolinium contrast agent) from the ATLAS dataset were acquired on five Siemens 3T and 1T MRI machines, this 3D

Methods	Type	DSC (%)			mIoU (%)		
		Liver	Tumor	Mean	Liver	Tumor	Mean
DoDNet	baseline	79.54	24.03	51.79	75.31	19.3	47.31
	ATLAS-PL	80.23	25.32	52.78	76.09	20.23	48.16
		+0.87%	+5.37%	+1.91%	+1.03%	+4.78%	+1.80%
MED3D	baseline	73.12	19.55	46.34	65.30	16.82	41.06
	ATLAS-PL	74.32	21.14	47.73	65.99	17.85	41.92
		+1.63%	+8.12%	+3.01%	+1.07%	+6.12%	+2.09%
SAM-Med2D	baseline	80.02	51.28	65.65	77.34	48.88	63.11
	ATLAS-PL	80.52	52.03	66.28	78.01	49.44	63.73
		+0.63%	+1.46%	+0.96%	+0.87%	+1.15%	+0.98%

Table 6: The ablation study of different area size thresholds.

MRI data is not directly applied to the vanilla SAM. To address this, we initially design a script to convert 3D MRI data into 2D PNG format, prior to implementing our framework for automatic annotation. The qualitative results are shown in Fig 5. From the visualization results, we can observe that our proposed framework, designed for 2D slices of MRI data, demonstrates effective segmentation of liver and kidney. Furthermore, the color mapping within the framework accurately corresponds to the designated colors (pink for kidney and blue for liver) across multiple images. Due to the weak texture feature information of images, there may be unrelated instances that have been assigned to error labels. However, the label assignment for primary instances also maintains higher accuracy.

To validate the pseudo-label ATLAS 2023 dataset (ATLAS-PL) we constructed, we selected mainstream methods for pre-training and fine-tuning, respectively. Specifically, we separately chose DoDNet (Zhang et al. 2021), MED3D (Chen, Ma, and Zheng 2019), and SAM-Med2D (Cheng et al. 2023a) for experimental validation. The experimental results are shown in Table 6, we can observe that after pre-training on our constructed ATLAS-PL, the performance of the above three methods has been significantly improved in both DSC and mIoU metrics. Specifically, for DoDNet, the DSC for Tumor increased by 5.37% and the mIoU by 4.78%. For MED3D, the DSC for Liver increased by 1.63%, and the mIoU by 1.07%. For SAM-Med2D, the increases in DSC and mIoU on average are 0.96% and 0.98%, respectively. We can attribute this signifi-

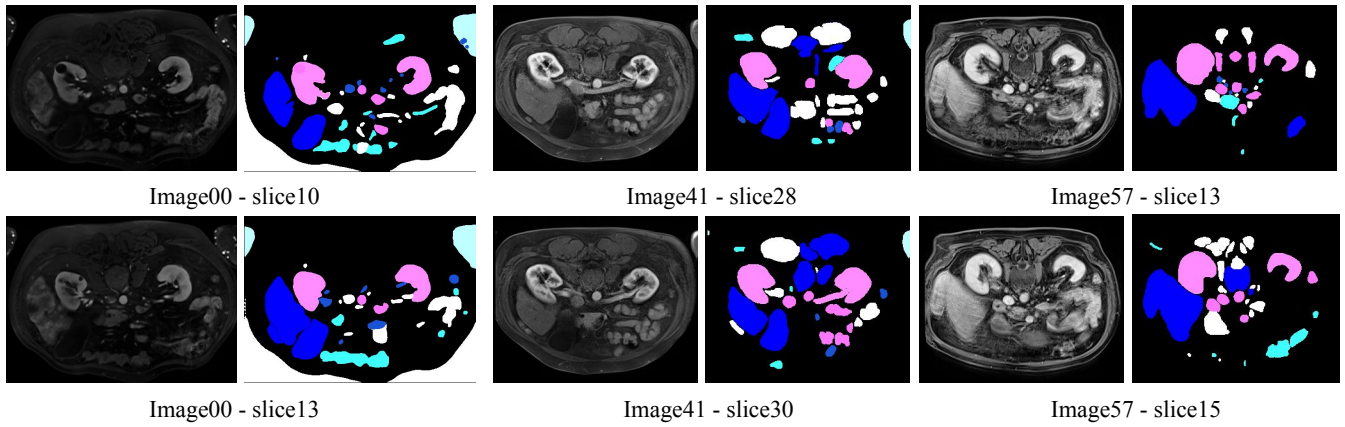


Figure 5: Some examples of Pseudo-Labeled results on ATLAS2023 dataset.

cant improvement to our proposed ALPS framework, which can fully utilize the ability of vanilla SAM and generalization of online K-means to predict pseudo-label without medical prior for later pre-training phrase.

Limitation and Consideration

In this study, our ALPS based vanilla SAM has been leveraged for data annotation tasks, demonstrating both time and cost efficiencies in processing extensive RS data. While our ALPS framework has successfully facilitated auto-labeling across a variety of segmentation tasks, it is imperative to acknowledge certain limitations that warrant further investigation:

(1) *Variability in Texture Features*: Instances within the same category may exhibit significant textural variation, potentially leading to diverse class assignments during feature clustering. Future research could explore the utilization of structured feature extraction to enhance clustering accuracy.

(2) *Dependency on SAM Segmentation*: The reliance on SAM for pseudo-labels introduces variability, such as the segmentation of a single object into multiple masks or the amalgamation of multiple objects into a single mask. This inconsistency can affect mask class association and the overall quality of the generated dataset. Future directions might include integrating DINO (Caron et al. 2021) to provide targeted information as prompts to SAM, aiming to refine mask predictions.

(3) *Novelty and Significance*: ALPS leverages the pre-trained SAM, which is originally trained on human-annotated data. However, in ALPS, no additional manual annotations are required for RS images, thus enabling a semi-automated annotation process without additional human intervention. Further, though every component in the pipeline has been well explored, the application of clustering algorithms in conjunction with SAM for RS images and the novel mechanism for aligning pseudo-labels represents a noteworthy adaptation and refinement for RS contexts. Finally, the individual performance improvements might appear marginal, however the cumulative effect across varying RS segmentation tasks highlights the robustness and gener-

alized enhancement provided by ALPS.

Conclusion

In conclusion, this paper introduces ALPS, an auto-labeling framework that capitalizes on the unmatched feature processing abilities of the vanilla Segment Anything Model (SAM) to efficiently annotate large-scale remote sensing (RS) datasets without additional prompts. Different from previous SAM extensions requiring additional detection prompts, ALPS adopts an innovative approach by extracting and clustering mask features to accurately predict PCL for each segmentation mask. To ascertain the efficacy of ALPS, we meticulously constructed two pseudo-labeled RS datasets, iSAID-PL and SAMRS-PL, without resorting to external annotations. Comprehensive experiments conducted on these datasets have underscored ALPS’s considerable impact on enhancing downstream task performances, establishing a new benchmark in the field. Furthermore, through rigorous ablation studies, the crucial role of mask class association and the incremental benefits of extending pre-training steps have been affirmed, attesting to the robustness and indispensability of each component within our framework. Marking a pioneering effort to employ SAM devoid of any prompts for auto-labeling, this study lays the groundwork for innovative feature clustering applications combined with computer vision foundation models. Our future work aim to explore the broader implications of our approach across different domains while striving to refine the precision of auto-labeling techniques further.

References

- Ball, J. E.; Anderson, D. T.; and Chan, C. S. 2017. Comprehensive survey of deep learning in remote sensing: theories, tools, and challenges for the community. *Journal of applied remote sensing*, 11(4): 042609–042609.
- Bearman, A.; Russakovsky, O.; Ferrari, V.; and Fei-Fei, L. 2016. What’s the point: Semantic segmentation with point supervision. In *European conference on computer vision*, 549–565. Springer.

- Blaschke, T.; Lang, S.; Lorup, E.; Strobl, J.; and Zeil, P. 2000. Object-oriented image processing in an integrated GIS/remote sensing environment and perspectives for environmental applications. *Environmental information for planning, politics and the public*, 2(1995): 555–570.
- Camps-Valls, G.; Tuia, D.; Gómez-Chova, L.; Jiménez, S.; and Malo, J. 2011. Remote sensing image processing.
- Cao, L.; Zhao, Z.; and Wang, D. 2023. Clustering algorithms. In *Target Recognition and Tracking for Millimeter Wave Radar in Intelligent Transportation*, 97–122. Springer.
- Caron, M.; Touvron, H.; Misra, I.; Jégou, H.; Mairal, J.; Bojanowski, P.; and Joulin, A. 2021. Emerging Properties in Self-Supervised Vision Transformers. In *Proceedings of the International Conference on Computer Vision (ICCV)*.
- Castellano, G.; Bonilha, L.; Li, L.; and Cendes, F. 2004. Texture analysis of medical images. *Clinical radiology*, 59(12): 1061–1069.
- Cen, J.; Zhou, Z.; Fang, J.; Shen, W.; Xie, L.; Jiang, D.; Zhang, X.; Tian, Q.; et al. 2024. Segment anything in 3d with nerfs. *Advances in Neural Information Processing Systems*, 36.
- Chen, K.; Liu, C.; Chen, H.; Zhang, H.; Li, W.; Zou, Z.; and Shi, Z. 2024. RSPrompter: Learning to prompt for remote sensing instance segmentation based on visual foundation model. *IEEE Transactions on Geoscience and Remote Sensing*.
- Chen, L.-C.; Zhu, Y.; Papandreou, G.; Schroff, F.; and Adam, H. 2018. Encoder-decoder with atrous separable convolution for semantic image segmentation. In *Proceedings of the European conference on computer vision (ECCV)*, 801–818.
- Chen, S.; Ma, K.; and Zheng, Y. 2019. Med3d: Transfer learning for 3d medical image analysis. *arXiv preprint arXiv:1904.00625*.
- Cheng, G.; Han, J.; and Lu, X. 2017. Remote sensing image scene classification: Benchmark and state of the art. *Proceedings of the IEEE*, 105(10): 1865–1883.
- Cheng, J.; Ye, J.; Deng, Z.; Chen, J.; Li, T.; Wang, H.; Su, Y.; Huang, Z.; Chen, J.; Jiang, L.; et al. 2023a. Sam-med2d. *arXiv preprint arXiv:2308.16184*.
- Cheng, Y.; Li, L.; Xu, Y.; Li, X.; Yang, Z.; Wang, W.; and Yang, Y. 2023b. Segment and track anything. *arXiv preprint arXiv:2305.06558*.
- Cho, J. H.; Mall, U.; Bala, K.; and Hariharan, B. 2021. Picie: Unsupervised semantic segmentation using invariance and equivariance in clustering. In *Proceedings of the IEEE/CVF Conference on Computer Vision and Pattern Recognition*, 16794–16804.
- Cohen-Addad, V.; Guedj, B.; Kanade, V.; and Rom, G. 2021. Online k-means clustering. In *International Conference on Artificial Intelligence and Statistics*, 1126–1134. PMLR.
- Contributors, M. 2020. MMSegmentation: OpenMMLab Semantic Segmentation Toolbox and Benchmark. <https://github.com/open-mmlab/mms Segmentation>.
- Dai, J.; He, K.; and Sun, J. 2015. Boxesup: Exploiting bounding boxes to supervise convolutional networks for semantic segmentation. In *Proceedings of the IEEE international conference on computer vision*, 1635–1643.
- Dechesne, C.; Mallet, C.; Le Bris, A.; and Gouet-Brunet, V. 2017. Semantic segmentation of forest stands of pure species as a global optimization problem. *ISPRS Annals of the Photogrammetry, Remote Sensing and Spatial Information Sciences*, 4: 141–148.
- Ding, J.; Xue, N.; Xia, G.-S.; Bai, X.; Yang, W.; Yang, M. Y.; Belongie, S.; Luo, J.; Datcu, M.; Pelillo, M.; et al. 2021. Object detection in aerial images: A large-scale benchmark and challenges. *IEEE transactions on pattern analysis and machine intelligence*, 44(11): 7778–7796.
- Dosovitskiy, A.; Beyer, L.; Kolesnikov, A.; Weissenborn, D.; Zhai, X.; Unterthiner, T.; Dehghani, M.; Minderer, M.; Heigold, G.; Gelly, S.; et al. 2020. An image is worth 16x16 words: Transformers for image recognition at scale. *arXiv preprint arXiv:2010.11929*.
- Fang, F.; Yuan, X.; Wang, L.; Liu, Y.; and Luo, Z. 2018. Urban land-use classification from photographs. *IEEE Geoscience and Remote Sensing Letters*, 15(12): 1927–1931.
- Fischer, P.; Azimi, S. M.; Roschlaub, R.; and Krauß, T. 2018. Towards HD maps from aerial imagery: Robust lane marking segmentation using country-scale imagery. *ISPRS International Journal of Geo-Information*, 7(12): 458.
- He, S.; Bao, R.; Li, J.; Grant, P. E.; and Ou, Y. 2023. Accuracy of segment-anything model (sam) in medical image segmentation tasks. *arXiv preprint arXiv:2304.09324*.
- Hong, S.; Noh, H.; and Han, B. 2015. Decoupled deep neural network for semi-supervised semantic segmentation. *Advances in neural information processing systems*, 28.
- Hou, Q.; Cheng, M.-M.; Hu, X.; Borji, A.; Tu, Z.; and Torr, P. H. 2017. Deeply supervised salient object detection with short connections. In *Proceedings of the IEEE conference on computer vision and pattern recognition*, 3203–3212.
- Hwang, J.-J.; Yu, S. X.; Shi, J.; Collins, M. D.; Yang, T.-J.; Zhang, X.; and Chen, L.-C. 2019. Segsort: Segmentation by discriminative sorting of segments. In *Proceedings of the IEEE/CVF International Conference on Computer Vision*, 7334–7344.
- Jadhav, J. K.; and Singh, R. 2018. Automatic semantic segmentation and classification of remote sensing data for agriculture. *Mathematical Models in Engineering*, 4(2): 112–137.
- Ji, X.; Henriques, J. F.; and Vedaldi, A. 2019. Invariant information clustering for unsupervised image classification and segmentation. In *Proceedings of the IEEE/CVF international conference on computer vision*, 9865–9874.
- Julka, S.; and Granitzer, M. 2023. Knowledge distillation with Segment Anything (SAM) model for Planetary Geological Mapping. *arXiv preprint arXiv:2305.07586*.
- Khoreva, A.; Benenson, R.; Hosang, J.; Hein, M.; and Schiele, B. 2017. Simple does it: Weakly supervised instance and semantic segmentation. In *Proceedings of the IEEE conference on computer vision and pattern recognition*, 876–885.

- Kirillov, A.; Mintun, E.; Ravi, N.; Mao, H.; Rolland, C.; Gustafson, L.; Xiao, T.; Whitehead, S.; Berg, A. C.; Lo, W.-Y.; et al. 2023. Segment anything. *arXiv preprint arXiv:2304.02643*.
- Kussul, N.; Lavreniuk, M.; Skakun, S.; and Shelestov, A. 2017. Deep learning classification of land cover and crop types using remote sensing data. *IEEE Geoscience and Remote Sensing Letters*, 14(5): 778–782.
- Li, H.; Xiong, P.; Fan, H.; and Sun, J. 2019. Dfanet: Deep feature aggregation for real-time semantic segmentation. In *Proceedings of the IEEE/CVF conference on computer vision and pattern recognition*, 9522–9531.
- Li, K.; Wan, G.; Cheng, G.; Meng, L.; and Han, J. 2020. Object detection in optical remote sensing images: A survey and a new benchmark. *ISPRS journal of photogrammetry and remote sensing*, 159: 296–307.
- Li, W.; Chen, Y.; Hu, K.; and Zhu, J. 2022. Oriented reppoints for aerial object detection. In *Proceedings of the IEEE/CVF conference on computer vision and pattern recognition*, 1829–1838.
- Lin, D.; Dai, J.; Jia, J.; He, K.; and Sun, J. 2016. Scribble-sup: Scribble-supervised convolutional networks for semantic segmentation. In *Proceedings of the IEEE conference on computer vision and pattern recognition*, 3159–3167.
- Lin, T.-Y.; Maire, M.; Belongie, S.; Hays, J.; Perona, P.; Ramanan, D.; Dollár, P.; and Zitnick, C. L. 2014. Microsoft coco: Common objects in context. In *Computer Vision—ECCV 2014: 13th European Conference, Zurich, Switzerland, September 6–12, 2014, Proceedings, Part V 13*, 740–755. Springer.
- Liu, Z.; Lin, Y.; Cao, Y.; Hu, H.; Wei, Y.; Zhang, Z.; Lin, S.; and Guo, B. 2021. Swin transformer: Hierarchical vision transformer using shifted windows. In *Proceedings of the IEEE/CVF international conference on computer vision*, 10012–10022.
- Liu, Z.; Yuan, L.; Weng, L.; and Yang, Y. 2017. A high resolution optical satellite image dataset for ship recognition and some new baselines. In *International conference on pattern recognition applications and methods*, volume 2, 324–331. SciTePress.
- Nassar, A.; Amer, K.; ElHakim, R.; and ElHelw, M. 2018. A deep CNN-based framework for enhanced aerial imagery registration with applications to UAV geolocalization. In *Proceedings of the IEEE conference on computer vision and pattern recognition workshops*, 1513–1523.
- [Online]. ????. Isprs.2d semantic labeling contest-potsdam. In Available: <http://www2.isprs.org/commissions/comm3/wg4/2d-sem-label-potsdam.html>.
- Papandreou, G.; Chen, L.-C.; Murphy, K. P.; and Yuille, A. L. 2015. Weakly-and semi-supervised learning of a deep convolutional network for semantic image segmentation. In *Proceedings of the IEEE international conference on computer vision*, 1742–1750.
- Pathak, D.; Krahenbuhl, P.; and Darrell, T. 2015. Constrained convolutional neural networks for weakly supervised segmentation. In *Proceedings of the IEEE international conference on computer vision*, 1796–1804.
- Pluim, J. P.; Maintz, J. A.; and Viergever, M. A. 2003. Mutual-information-based registration of medical images: a survey. *IEEE transactions on medical imaging*, 22(8): 986–1004.
- Quinton, F.; Popoff, R.; Presles, B.; Leclerc, S.; Meriaudeau, F.; Nodari, G.; Lopez, O.; Pellegrinelli, J.; Chevallier, O.; Ginhac, D.; et al. 2023. A tumour and liver automatic segmentation (atlas) dataset on contrast-enhanced magnetic resonance imaging for hepatocellular carcinoma. *Data*, 8(5): 79.
- Ren, S.; Luzi, F.; Lahrachi, S.; Kassaw, K.; Collins, L. M.; Bradbury, K.; and Malof, J. M. 2024. Segment anything, from space? In *Proceedings of the IEEE/CVF Winter Conference on Applications of Computer Vision*, 8355–8365.
- Ronen, M.; Finder, S. E.; and Freifeld, O. 2022. Deepdpm: Deep clustering with an unknown number of clusters. In *Proceedings of the IEEE/CVF Conference on Computer Vision and Pattern Recognition*, 9861–9870.
- Rottensteiner, F.; Sohn, G.; Jung, J.; Gerke, M.; Baillard, C.; Benitez, S.; and Breitkopf, U. 2012. The ISPRS benchmark on urban object classification and 3D building reconstruction. *ISPRS Annals of the Photogrammetry, Remote Sensing and Spatial Information Sciences; I-3*, 1(1): 293–298.
- Strudel, R.; Garcia, R.; Laptev, I.; and Schmid, C. 2021. Segmenter: Transformer for semantic segmentation. In *Proceedings of the IEEE/CVF international conference on computer vision*, 7262–7272.
- Sun, X.; Wang, P.; Yan, Z.; Xu, F.; Wang, R.; Diao, W.; Chen, J.; Li, J.; Feng, Y.; Xu, T.; et al. 2022. FAIR1M: A benchmark dataset for fine-grained object recognition in high-resolution remote sensing imagery. *ISPRS Journal of Photogrammetry and Remote Sensing*, 184: 116–130.
- Tang, M.; Djelouah, A.; Perazzi, F.; Boykov, Y.; and Schroers, C. 2018a. Normalized cut loss for weakly-supervised cnn segmentation. In *Proceedings of the IEEE conference on computer vision and pattern recognition*, 1818–1827.
- Tang, M.; Perazzi, F.; Djelouah, A.; Ben Ayed, I.; Schroers, C.; and Boykov, Y. 2018b. On regularized losses for weakly-supervised cnn segmentation. In *Proceedings of the European Conference on Computer Vision (ECCV)*, 507–522.
- Tuia, D.; Ratle, F.; Pacifici, F.; Kanevski, M. F.; and Emery, W. J. 2009. Active learning methods for remote sensing image classification. *IEEE Transactions on Geoscience and Remote Sensing*, 47(7): 2218–2232.
- Van Gansbeke, W.; Vandenhende, S.; Georgoulis, S.; and Van Gool, L. 2021. Unsupervised semantic segmentation by contrasting object mask proposals. In *Proceedings of the IEEE/CVF International Conference on Computer Vision*, 10052–10062.
- Vernaza, P.; and Chandraker, M. 2017. Learning random-walk label propagation for weakly-supervised semantic segmentation. In *Proceedings of the IEEE conference on computer vision and pattern recognition*, 7158–7166.

- Volpi, M.; and Ferrari, V. 2015. Semantic segmentation of urban scenes by learning local class interactions. In *Proceedings of the IEEE Conference on Computer Vision and Pattern Recognition Workshops*, 1–9.
- Wang, D.; Zhang, J.; Du, B.; Xu, M.; Liu, L.; Tao, D.; and Zhang, L. 2024. SAMRS: Scaling-up remote sensing segmentation dataset with segment anything model. *Advances in Neural Information Processing Systems*, 36.
- Wang, J.; Sun, K.; Cheng, T.; Jiang, B.; Deng, C.; Zhao, Y.; Liu, D.; Mu, Y.; Tan, M.; Wang, X.; et al. 2020. Deep high-resolution representation learning for visual recognition. *IEEE transactions on pattern analysis and machine intelligence*, 43(10): 3349–3364.
- Waqas Zamir, S.; Arora, A.; Gupta, A.; Khan, S.; Sun, G.; Shahbaz Khan, F.; Zhu, F.; Shao, L.; Xia, G.-S.; and Bai, X. 2019. isaid: A large-scale dataset for instance segmentation in aerial images. In *Proceedings of the IEEE/CVF Conference on Computer Vision and Pattern Recognition Workshops*, 28–37.
- Wu, J.; Xu, R.; Wood-Doughty, Z.; and Wang, C. 2023. Segment anything model is a good teacher for local feature learning. *arXiv preprint arXiv:2309.16992*.
- Xiao, T.; Liu, Y.; Zhou, B.; Jiang, Y.; and Sun, J. 2018. Unified perceptual parsing for scene understanding. In *Proceedings of the European conference on computer vision (ECCV)*, 418–434.
- Xie, E.; Wang, W.; Yu, Z.; Anandkumar, A.; Alvarez, J. M.; and Luo, P. 2021. SegFormer: Simple and efficient design for semantic segmentation with transformers. *Advances in Neural Information Processing Systems*, 34: 12077–12090.
- Xu, J.; Schwing, A. G.; and Urtasun, R. 2015a. Learning to segment under various forms of weak supervision. In *Proceedings of the IEEE conference on computer vision and pattern recognition*, 3781–3790.
- Xu, J.; Schwing, A. G.; and Urtasun, R. 2015b. Learning to segment under various forms of weak supervision. In *Proceedings of the IEEE conference on computer vision and pattern recognition*, 3781–3790.
- Xu, R.; and Wunsch, D. 2005. Survey of clustering algorithms. *IEEE Transactions on neural networks*, 16(3): 645–678.
- Yang, S.; Chen, Q.; Yuan, X.; and Liu, X. 2016. Adaptive coherency matrix estimation for polarimetric SAR imagery based on local heterogeneity coefficients. *IEEE Transactions on Geoscience and Remote Sensing*, 54(11): 6732–6745.
- Yu, C.; Wang, J.; Peng, C.; Gao, C.; Yu, G.; and Sang, N. 2018. Learning a discriminative feature network for semantic segmentation. In *Proceedings of the IEEE conference on computer vision and pattern recognition*, 1857–1866.
- Yuan, X.; and Sarma, V. 2010. Automatic urban water-body detection and segmentation from sparse ALSM data via spatially constrained model-driven clustering. *IEEE Geoscience and Remote Sensing Letters*, 8(1): 73–77.
- Zhang, J.; Xie, Y.; Xia, Y.; and Shen, C. 2021. Dodnet: Learning to segment multi-organ and tumors from multiple partially labeled datasets. In *Proceedings of the IEEE/CVF conference on computer vision and pattern recognition*, 1195–1204.
- Zhang, J.; Zhou, Z.; Mai, G.; Mu, L.; Hu, M.; and Li, S. 2023. Text2Seg: Remote Sensing Image Semantic Segmentation via Text-Guided Visual Foundation Models. *arXiv preprint arXiv:2304.10597*.
- Zhang, X.; and Maire, M. 2020. Self-supervised visual representation learning from hierarchical grouping. *Advances in Neural Information Processing Systems*, 33: 16579–16590.
- Zhang, Z.; Zhang, X.; Peng, C.; Xue, X.; and Sun, J. 2018. Exfuse: Enhancing feature fusion for semantic segmentation. In *Proceedings of the European conference on computer vision (ECCV)*, 269–284.
- Zhao, H.; Shi, J.; Qi, X.; Wang, X.; and Jia, J. 2017. Pyramid scene parsing network. In *Proceedings of the IEEE conference on computer vision and pattern recognition*, 2881–2890.
- Zhou, Y.; Yang, X.; Zhang, G.; Wang, J.; Liu, Y.; Hou, L.; Jiang, X.; Liu, X.; Yan, J.; Lyu, C.; Zhang, W.; and Chen, K. 2022. MMRotate: A Rotated Object Detection Benchmark using PyTorch. In *Proceedings of the 30th ACM International Conference on Multimedia*.